Electromechanical Actuator with Controllable Motion, Fast Response Rate, and High-Frequency Resonance Based on Graphene and Polydiacetylene

Jiajie Liang,[†] Lu Huang,[†] Na Li,[†] Yi Huang,[†,*] Yingpeng Wu,[†] Shaoli Fang,[‡] Jiyoung Oh,[‡] Mikhail Kozlov,[‡] Yanfeng Ma,[†] Feifei Li,[†] Ray Baughman,[‡] and Yongsheng Chen[†,*]
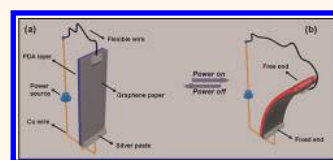
[†]Key Laboratory of Functional Polymer Materials and Centre for Nanoscale Science and Technology, Institute of Polymer Chemistry, College of Chemistry, Nankai University, 300071, Tianjin, China and [‡]Alan G. MacDiarmid NanoTech Institute, University of Texas at Dallas, Richardson, Texas 75083, United States

Electromechanical actuators, which can directly convert electrical energy to mechanical energy through a material mechanical response, have been continuing to grab considerable attention for a variety of practical applications and technological uses, including sensitive switches, artificial muscle, microrobotics, optical display, prosthetic devices, and even microscopic pumps.[1−6] In most cases, ferroelectric ceramics, electroactive polymers (EAPs), and conventional conjugated conducting polymers (CPs) have been investigated and widely utilized as actuator materials owing to their direct energy conversion. These traditional electromechanical actuator materials excel in some actuation performance, such as high energy density for ferroelectric ceramics,[7,8] large actuation strain for EPAs,[2,9,10] and low activated voltages for conjugated CPs.[1,3,11,12] Nevertheless, they may still be unsatisfactory in other areas, i.e., small actuation strain for ferroelectric ceramics, high driving voltages for EPAs, limiting cycle life, and response rate for conjugated CPs. To date, these drawbacks still pose significant hurdles for many practical applications of conventional electromechanical actuators.

Diacetylene and its polymer polydiacetylene (PDA, Scheme S1) compose a very special class of molecular materials with interesting electrical and optical properties. PDA has been extensively investigated as a chromatic sensor material owing to its interesting blue-to-red color change (namely, "blue" phase to "red" phase transition), which can be actuated electrically, thermally, optically, chemically, and mechanically.[13−17] In particular, when environmental stimuli are applied to the "blue"

phase PDA (usually with an absorption maximum in the range around 640 nm),[16] the motional freedom of the pendant side groups on PDA will increase and cause a more disordered polymer structure. The changes of side-chain conformation strain the carbon backbone, lead to the optical absorption blue-shift of the PDA, and thus produce the "red" phase PDA (usually with

ABSTRACT Although widely investigated, novel electromechanical actuators with high overall actuation performance are still in urgent need for various practical and scientific applications, such as robots, prosthetic devices, sensor switches, and sonar projectors. In this work, combining the properties of unique environmental perturbations-actuated deformational isomerization of polydiacetylene (PDA) and the outstanding intrinsic features of graphene together for the first time, we design and fabricate an electromechanical bimorph actuator composed of a layer of PDA crystal and a layer of flexible graphene paper through a simple yet versatile solution approach. Under low applied direct current (dc), the graphene—PDA bimorph actuator with strong mechanical strength can generate large actuation motion (curvature is about 0.37 cm^{-1} under a current density of 0.74 A/mm^2) and produce high actuation stress (more than 160 MPa/g under an applied dc of only 0.29 A/mm^2). When applying alternating current (ac), this actuator can display reversible swing behavior with long cycle life under high frequencies even up to 200 Hz; significantly, while the frequency and the value of applied ac and the state of the actuators reach an appropriate value, the graphene—PDA actuator can produce a strong resonance and the swing amplitude will jump to a peak value. Moreover, this stable graphene—PDA actuator also demonstrates rapidly and partially reversible electrochromatic phenomenon when applying an ac. Two mechanisms—the dominant one, electric-induced deformation, and a secondary one, thermal-induced expansion of PDA—are proposed to contribute to these interesting actuation performances of the graphene—PDA actuators. On the basis of these results, a mini-robot with controllable direction of motion based on the graphene—PDA actuator is designed to illustrate the great potential of our discoveries for practical use. Combining the unique actuation mechanism and many outstanding properties of graphene and PDA, this novel kind of graphene—PDA actuator exhibits compelling advantages to traditional electromechanical actuation technology and may provide a new avenue for actuation applications.

KEYWORDS: electromechanical actuator · graphene · polydiacetylene · resonance · electrochromatic

an absorption peak in the range of approximate 540 nm).[13−16] This deformational isomerization of the side groups is the scientific foundation for the new generation of mechanical actuators exploiting PDA materials. Ikehara and co-workers[18] first reported that the anisotropic thermal strain of a bulk PDA crystal induced *via* a heat cycle could be measured from macroscopic changes in the sample dimensions. This attractive deformation was supposed to be used for mechanical actuation. Subsequently, Ikehara proposed a new optically driven actuator, which utilized the photoactive nature of PDA material that exhibited photoinduced phase transitions.[19] Recently, by incorporation of carbon nanotube (CNT) fibers as a matrix to make PDA−CNT nanocomposite fibers, Peng and co-workers reported the first change of "blue" phase to "red" phase for PDA, actuated through an electric current.[20] These pioneering works[18−20] indicate that PDA has great potential to be used for various actuation applications, which can be triggered *via* different stimuli including electrical energy. Unfortunately, despite these early successes, the shortcomings of poor processability and difficulty of forming standalone bulk film materials using pure PDA are severely handicapping its practical use in the field of actuation. Therefore, effective approaches that can overcome the intrinsic drawbacks of PDA and bring PDA's actuation characteristics into full play are highly needed to construct high-performance PDA-based electromechanical actuators.

The new electromechanical actuator we describe here is a bimorph actuator that is composed of a layer of PDA crystal and a layer of flexible graphene paper. Graphene, a one atom thick and two-dimensional (2D) single layer, has attracted enormous attention in the field of material science due to its intrinsic prominent electrical, thermal, and mechanical properties and unusual structural features,[21−25] which may rival or even surpass both single-walled and multiwalled carbon nanotubes. These excellent and unique properties make this highly versatile carbon material extraordinarily promising in many potential applications.[26−30] Particularly, the graphene-based paper-like materials prepared through a simple solution process not only can preserve the superb mechanical, electrical, and thermal properties of graphene at a great degree but also exhibit low weight and excellent flexibility,[28,31,32] which are highly demanded properties for a range of scientific frontiers or multifunctional applications,[28,31,32] such as high-performance actuators.[33−38] For instance, Park *et al*. prepared a graphene oxide/carbon nanotube bilayer paper that revealed a curling actuation behavior depending on humidity and/ozr temperature.[37] Recently, Xie *et al*., Rogers *et al*., and our recent work also demonstrated the electrochemical actuation of graphene-based paper with an actuation mechanism dominated by quantum chemical expansion due

to electrochemical double-layer charging.[33,35,38] Importantly, Zhu *et al*. developed an electromechanically driven microactuator based on a graphene-on-epoxy film hybrid bimorph, and an intriguing large displacement with rapid response was observed for this microactuator at low input power.[36] These pioneering works indicate that graphene has great potential to be applied in high-performance actuators, especially electromechanical actuators, which are still exceptional in meeting the high demand of practical and scientific use. Herein, exploiting the synergism between unique PDA materials and flexible graphene paper, we report for the first time an electromechanical graphene−PDA bimorph actuator with excellent performance. When applying only a low direct current (dc) or current density, the flexible graphene−PDA actuator can perform large and controllable actuation bending motion (curvature reach about 0.37 cm^{-1} under a current density of 0.74 A/mm^2) and is able to generate higher actuation stress than natural muscles (more than 160 MPa/g under an applied dc of only 0.29 A/mm^2). Moreover, this stable actuator also demonstrates a rapidly and partially reversible electrochromic phenomenon when applying an alternating current (ac). Of great significance is that when applying ac, this actuator, which has an ultrafast response rate, can display reversible and reliable swing behavior with high frequencies (even up to 200 Hz); while reaching appropriate conditions, the actuator is able to produce intriguing resonance phenomena. It is proposed that this novel and striking actuation performance is a result of the effective combination of the remarkable features of graphene and an electric-induced as well as thermal-induced expansion mechanism of the PDA crystal. On this basis, a graphene−PDA actuator-based mini-robot with controllable direction of movement is designed to illustrate the great potential of our discoveries in practical use.

RESULT AND DISCUSSION

Structure Characterization of Graphene−PDA Bimorph Actuator. Free-standing and shiny black graphene papers, as depicted in Figure S1(a), are readily fabricated through vacuum filtering of the homogeneous graphene solution, followed by 400 °C annealing according to previous works.[31,32,39] As already widely explored, this free-standing graphene paper possessed with excellent flexibility, high conductivity, and good mechanical strength.[1,31,38] For example, it has been reported that the electrical conductivity and mechanical strength can reach as high as 100 S/cm and 100 MPa orders of magnitude.[31] In addition, graphene paper keeps its high flexibility, and no visible breakage or decreasing performance was observed for the graphene paper after more than hundreds of bending cycles with bending to angles larger than 90°.[32] More importantly, the unique large-scale two-dimension structure of
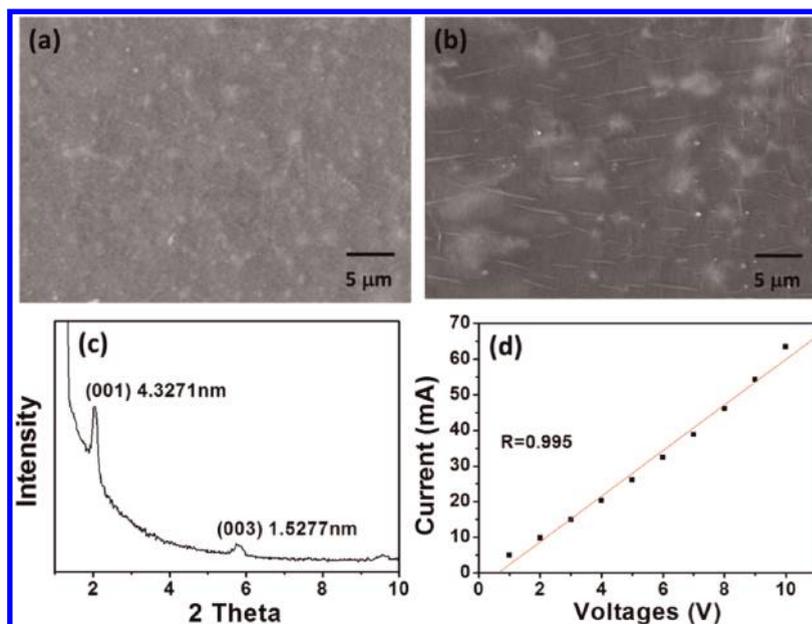
Figure 1. (a) Top-view SEM image of pure graphene paper. (b) Top-view SEM image of PDA crystal layer on the graphene−PDA paper. (c) XRD pattern of PDA crystal layer on the graphene−PDA paper. (d) Current−voltage ($I−V$) curve of the graphene−PDA bimorph actuator. The correlation factor R of the linear line is 0.995.

graphene also gives the graphene paper a relatively smooth surface (Figure 1a), which is difficult to achieve by one-dimensional carbon nanotubes and zero-dimensional nanoparticles. These combined outstanding features thus made graphene paper an excellent choice for fabricating overall high-performance actuators.[1,38] A representative side-view SEM image of the cross-section of a graphene paper is exhibited in Figure S1(b); a well-packed layered structure can be clearly seen, and the thickness of the graphene paper is about 10 μm. Making use of this graphene paper as a matrix, a graphene−PDA bimorph actuator was fabricated by directly coating a tetrahydrofuran solution of 10,12-pentacosadiynoic acid monomer (one of the most commonly used diacetylene precursors for PDA) on one side of the graphene paper, followed by photopolymerization under 254 nm UV radiation (see Methods for details). It is interesting to note that the PDA side of the bimorph paper is dark blue, which is visible to the unaided eye (Figure S1(c)) and can be characterized by a UV−vis spectrum measured using solid reflection UV directly, as will be discussed in detail below. As shown in Figure 1b, SEM analyses from the top view of the PDA side for the graphene−PDA bimorph paper reveal that a well-ordered striped structure of PDA in long-range order can be clearly found on the surface of the graphene paper. In addition, the XRD pattern (Figure 1c) also depicts that the PDA layer on the surface of the graphene paper shows a lamellar crystal structure with a (001) diffraction peak at about 4.3 nm and a (003) diffraction peak at around 1.5 nm.[40] Hence, the PDA layer adhered on the surface of graphene paper possesses a crystalline structure.[40]

The structures of the PDA crystal and graphene−PDA bimorph paper are also characterized by FT-IR and Raman spectra, as shown in Figures S2 and S3. Moreover, the graphene−PDA actuator exhibits a good conductivity of about 3000−5000 S/m. While the conductivity of pure PDA is estimated to be lower than 10^{-4} S/m,[41] the high conductivity of the actuator mainly arises from the graphene paper. Figure 1d further displays the current−voltage ($I−V$) curve of the graphene−PDA actuator. The linear line of the data with a correlation factor R of about 0.995 indicates an ideal ohmic behavior of our actuator.[42]

Actuation Performance of Graphene−PDA Bimorph Actuator When Passing dc. For the sake of investigating the actuation performance of the graphene−PDA actuator, a homemade experimental setup was designed and is demonstrated in Figure 2. As can be seen in the schematic illustration (Figure 2a), one end of the graphene−PDA actuator was fixed to an electrode of Cu wire; the other end of the actuator was connected with a conductive wire using a flexible CNT fiber. Accordingly, when the graphene−PDA actuator was exposed to dc, the end connected to the Cu wire was fixed and cannot move; in contrast, the end connected with the flexible CNT fiber can move freely and the actuator would bend to the side of the graphene paper (Figure 2b and Scheme S4 (see Supporting Information)). We have also tried other materials such as Au wire for the flexible conductive wire connected to the free end, but the point is to get both high conductivity and flexibility to obtain the intrinsic performance of the actuator accurately. Thus, due to the high flexibility, high conductivity, and light weight, the CNT fiber gave
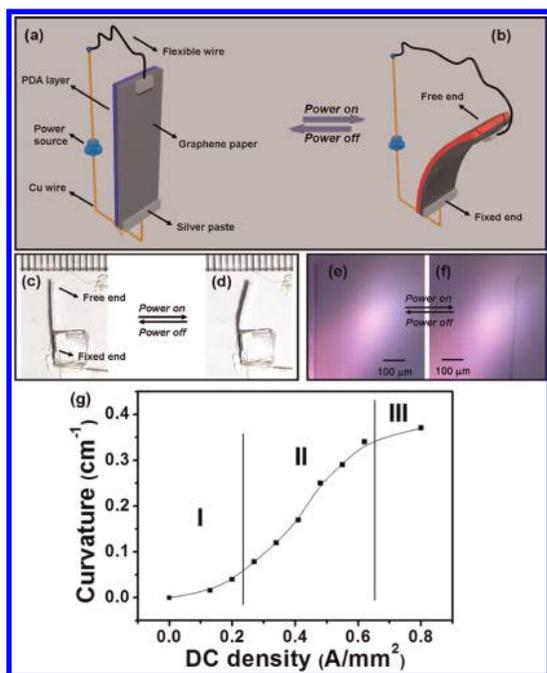
Figure 2. Schematic illustration of the bending actuation for the graphene−PDA actuator without (a) and with (b) an applied dc. Optical photos of the bending actuation for the graphene−PDA bimorph actuator (10 mm × 2.7 mm × 10 μm) without (c) and with (d) an applied dc of 20 mA (current density about 0.74 A/mm^2). The unit of the ruler is 1 mm. Optical microscope photos of the movable end of the graphene−PDA actuator without (e) and with (f) an applied dc of 7.5 mA (current density about 0.28 A/mm^2). The bending actuation is highly reversible. (g) Applied dc density dependence of the maximum curvature for the graphene−PDA bimorph actuator (10 mm × 2.7 mm × 10 μm). The curvature−current curve can be divided into three regions (region I, region II, and region III).

the best results. Figure 2c and d show optical photos of the graphene−PDA actuator without and with an applied dc. As displayed in Figure 2d, the graphene−PDA bimorph paper is actuated and the free end of the actuator bends to the graphene side under an applied dc. When the applied dc is only about 20 mA (density about 0.74 A/mm^2), the displacement and curvature achieved by the graphene−PDA actuator (length by width = 10 mm by 2.7 mm) are as large as 1.8 mm and 0.37 cm^{-1}, respectively, as shown in Figure 2d. An optical microscope coupled with a CCD camera is used to record and characterize this actuation movement of the graphene−PDA actuator, as demonstrated in Figure 2e and f. As noted in Figure 2g, the curvature of the graphene−PDA actuator is increased by increasing the value of the current density, which will be further discussed below.

The electric-induced stress of a series of three graphene−PDA actuators with different loadings of PDA (11.1 wt % for graphene−PDA-1, 20.0 wt % for graphene−PDA-2, and 33.3 wt % for graphene−PDA-3 paper, as shown in Table 1) is investigated, and the results are depicted in Figure 3. An experimental setup, as demonstrated in Figure S4, was designed and utilized to measure the generated stress for the actuators. The graphene−PDA actuator was fixed at one end to an adjustable inching lab jack and connected at the opposite end to the pan of a precision balance, as detailed in the Methods. The dimensions of the graphene−PDA actuator chosen in this measurement of electric-induced stress are about 25 mm × 4 mm (length × width) with a thickness of 10−13 μm, which

TABLE 1. PDA Contents of a Series of Graphene−PDA Bimorph Actuators

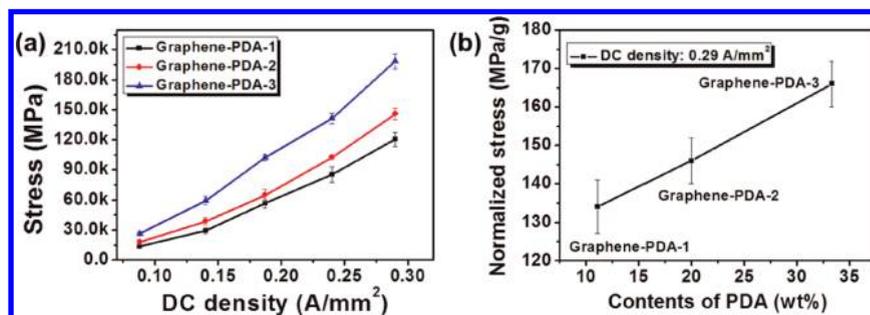|	dimensions (length by width)						
	25 mm × 4 mm				10 mm × 2.7 mm		
sample	graphene−PDA-1	graphene−PDA-2	graphene−PDA-3	graphene−PDA-4	graphene−PDA-5	graphene−PDA-6	graphene−PDA-7
contents of PDA (wt %)	11.1	20.0	33.3	9.1	16.7	28.6	37.5

Figure 3. (a) Current density *vs* the generated stress for three graphene−PDA actuators with different loadings of PDA (11.1 wt % for graphene−PDA-1, 20.0 wt % for graphene−PDA-2, and 33.3 wt % for graphene−PDA-3); the dimensions of these three samples are about 25 mm × 4 mm (length × width), with a thickness of around 10−13 μm (see Table 1). (b) Specific normalized stress generated by three graphene−PDA actuators (graphene−PDA-1, graphene−PDA-2, and graphene−PDA-3 actuators) at an applied dc density of 0.29 A/mm^2 (the applied current is about 11.5 mA).
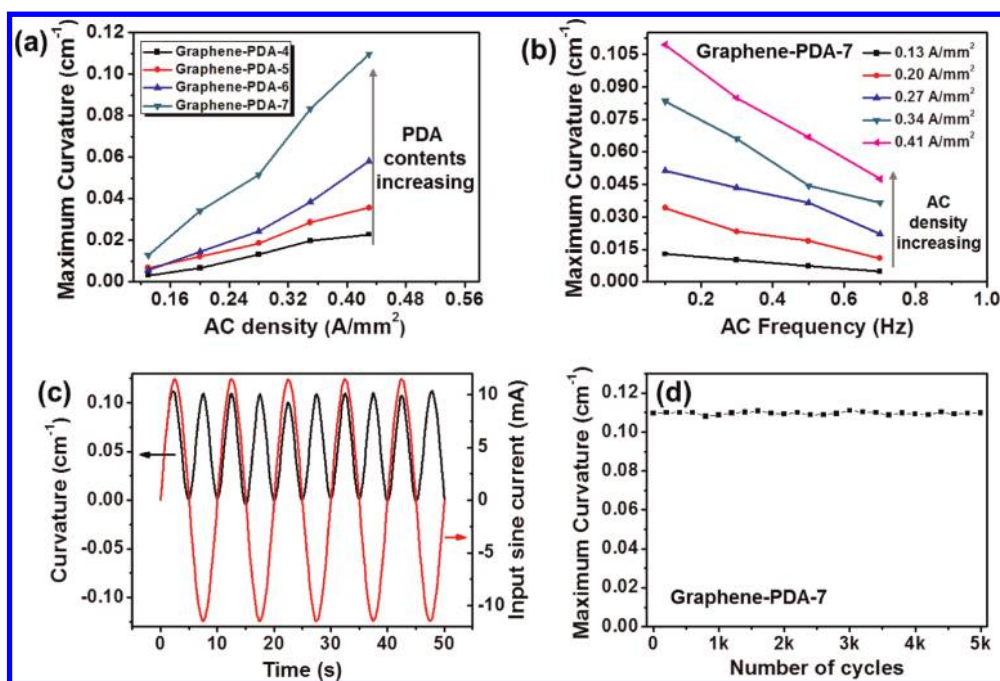
Figure 4. (a) Current density dependence of the maximum actuation curvature for four graphene−PDA actuators with different contents of PDA (9.1 wt % for graphene−PDA-4, 16.7 wt % for graphene−PDA-5, 28.6 wt % for graphene−PDA-6, and 37.5 wt % for graphene−PDA-7 actuators) under 0.1 Hz ac; the dimensions of these four samples are about 10 mm × 2.7 mm (length × width) with a thickness of around 10−13 μm (see Table 1). (b) Maximum actuation curvature of the graphene−PDA-7 actuator as a function of frequency for a series of applied sine wave currents. (c) Curvature vibration of the graphene−PDA-7 actuator with a 0.1 Hz sine wave alternating current of ±11.5 mA (ac density about ±0.43 A/mm²). (d) Cycle life testing of the graphene−PDA-7 actuator with a 0.1 Hz sine wave alternating current of ±11.5 mA (ac density about ±0.43 A/mm²) for 5000 cycles. The experimental setup is the same as displayed in Figure 2a.

is selected to match our homemade experimental setup for convenient measurement. Before carrying out the actuation stress measurement for all actuator samples, the inching lab jack was tuned to preload a force of about 0.0196 N on the graphene−PDA actuator to make sure that the papers were vertical to the horizontal plane of the balance. The electric-induced stress is performed utilizing dc, and the obtained force is normalized by the thickness of the graphene−PDA actuator, as shown in Figure 3a. The generated stress is increased with an increase of the applied dc density as well as the loadings of PDA in the actuators. Moreover, the generated stress up to about 0.2 MPa is achieved for the graphene−PDA-3 actuator under an applied dc density of 0.29 A/mm². In principal, if applying a higher dc (i.e., larger than 0.74 A/mm² dc density for graphene−PDA-3) or coating with more PDA, the generated stress for the graphene−PDA bimorph actuator (with mass only about 1−2 mg) should be larger than the peak capacity of human skeletal muscle (∼0.4 MPa).[1] Remarkably, the generated specific stress (normalized by the mass of the total actuator samples) for graphene−PDA-3 paper can reach more than 160 MPa/g under an applied dc of only 0.29 A/mm² (as displayed in Figure 3b), which is larger than the tensile strength of many kinds of traditional engineering polymer materials.

Actuation Performance of Graphene−PDA Bimorph Actuator When Applying Low-Frequency ac. When applying low-frequency ac,

the graphene−PDA actuators can be triggered and exhibit rapid and reversible swing motion, as demonstrated in Figure 4 (supplementary movie 1, see Supporting Information). The experimental setup is the same as displayed in Figure 2a. A series of four samples with different loadings of PDA (9.1 wt % for graphene−PDA-4, 16.7 wt % for graphene−PDA-5, 28.6 wt % for graphene−PDA-6, and 37.5 wt % for graphene−PDA-7 actuators, as shown in Table 1) are prepared for comparison and investigation, and the dimensions of the actuators are approximate 10 mm × 2.7 mm (length × width) with a thickness of 10−13 μm. The dimensional sizes of the graphene−PDA actuators were selected to match the experimental setup for convenient measurement, as shown in Figure 2. The 0.1 Hz ac density dependence of the maximum actuation curvature for the four graphene−PDA actuators is first tested as displayed in Figure 4a. Note that the maximum actuation curvature for all four samples is enhanced nearly linearly with the increase of input ac density; in addition, higher loadings of PDA induce better actuation performance (Figure 4a). Furthermore, it can be clearly seen in Figure 4b that the maximum curvature or maximum displacement decreases with an increase of the ac driving frequency: large curvature can be observed at low frequency, and small curvature occurs under relatively high frequency.[43,44] This phenomenon may be attributed to the relatively slow rate of

conformational changes of PDA. While charging at dc or low-frequency ac, PDA could have enough time to achieve its maximum conformational changes; however, when applying high-frequency ac, the rate of conformational changes of PDA may lag behind the charging rate, resulting in insufficient deformational isomerization of PDA. Therefore, the electromechanical actuation motion of our graphene—PDA bimorph actuators can be easily controlled through tuning the loadings of PDA, the values of applied ac (or ac density), and the frequencies of applied ac. Additionally, the frequency of the actuator swing (Figure 4c), consistent with the spectrum change of PDA (Figure 7e and f, as will be discussed below), is twice the frequencies of the applied ac wave, indicating the response rate of our graphene—PDA actuators is rather fast and the bending behavior is irrelevant to the current direction.[44] Furthermore, the reliability and repeatability of the swing actuation performance for the actuator were also investigated. As demonstrated in Figure 4d, the graphene—PDA-7 actuator was tested for more than 5000 swing cycles with 0.1 Hz sine wave ac of ±11.5 mA (ac density about ±0.43 A/mm^2) continually, and no downgraded actuation performance was observed. Similar results are also obtained for other graphene—PDA actuators with different loadings of PDA. These results indicate that our graphene—PDA actuators are quite reversible and have long life cycles, which may be due to the excellent flexibility and mechanical strength of the graphene paper.

Actuation Performance of Graphene—PDA Bimorph Actuator When Applying High-Frequency ac. Importantly, this oscillation phenomenon can still be observed through an optical microscope even on applying high-frequency ac (supplementary movies 2 and 3; see Supporting Information). Moreover, when the frequency of the applied ac reaches an appropriate value, the graphene—PDA actuator can produce a strong resonance and the swing amplitude will jump to a peak value. As displayed in Figure 5a, while the frequency of applied ac (±0.58 A/mm^2 ac density) increases to 17 Hz, the graphene—PDA actuator with dimensions of about 9.0 mm $\times$ 1.2 mm (length $\times$ width) can produce resonance, and the tip displacement jumps to a striking peak value of about 4.8 mm under resonance frequency (Figure 5a, also can be seen in supplementary movies 2 and 3, Supporting Information). This tip placement under high frequency was measured by a high-speed camera (Casio EX-ZR100). Furthermore, it is worth noting that through controlling the dimensions of the graphene—PDA actuators and the value of the ac input, the resonance frequencies can be readily controlled, as depicted in Figure 5b. For instance, at a fixed size of the dimensions of the graphene—PDA actuator, the resonance frequency increases as the value of ac input decreases; at a fixed value of input ac, the graphene—PDA actuator with larger dimensions produces
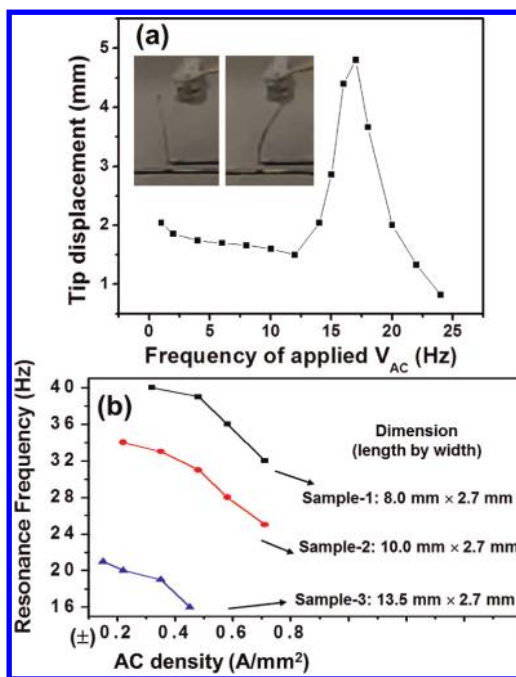

Figure 5. (a) Frequency of applied ac dependence of the tip displacement for the graphene—PDA actuators (dimensions are about 9.0 mm $\times$ 1.2 mm (length $\times$ width)) when applying a ±0.57 A/mm^2 ac density. Inset pictures: the movement of the tip measured by high-speed camera. (b) ac density dependence of the resonance frequency for graphene—PDA-7 actuators with three different dimensions (length $\times$ width): 8.0 mm $\times$ 2.7 mm (sample 1), 10.0 mm $\times$ 2.7 mm (sample 2), 13.5 mm $\times$ 2.7 mm (sample 3). The experimental setup is the same as displayed in Figure 2a.

resonance at lower frequency, and at a fixed frequency of the ac, the graphene—PDA actuator with larger dimensions can generate resonance below the lower value of the ac.

Mechanical resonance is the tendency of a physical system to absorb more energy and oscillate with larger amplitude when the frequency of the applied external stimulating forces matches the physical system's intrinsic resonant frequency of vibration than it does at other frequencies. Generally, for a given system, its intrinsic natural resonant frequency is also fixed, depending on only the system's intrinsic properties, such as the system's material, shape, size, and mechanical properties. Accordingly, when other factors are fixed, the physical system with larger size should have a lower natural frequency (namely, lower resonance frequency), which is consistent with the results shown in Figure 5b for graphene—PDA actuators. For our systems, as shown in Figure 2c and Figure 4a, due to the bimorph nature of graphene—PDA bimorph actuators, with different currents applied, perturbations (thermal and electric) on the PDA crystal layer (and probably the graphene layer too) would be different, leading to different actuation/bending curvature under different applied current density and thus different intrinsic resonant frequency. This indicates that the system's intrinsic parameters can be changed,
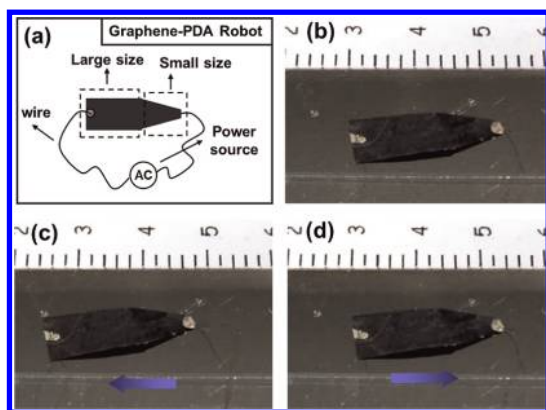
Figure 6. Design of a controllable mini-robot based on a graphene—PDA actuator. (a) Illustration of the structure of a controllable graphene—PDA actuator-based robot. The bimorph actuator consists of two parts with different dimensions. The large part is about 18 mm^2, and the small part is around 8 mm^2. (b) Optical image of a graphene—PDA actuator-based robot. (c) Optical image of a graphene—PDA actuator-based robot under ± 20 mA ac with 50 Hz frequency; the robot is moving back from right to left. (d) Optical image of a graphene—PDA actuator-based robot under ± 16 mA ac with 50 Hz frequency; the robot is moving from left to right.

different from the purely mechanical systems. As a result, for a given graphene—PDA actuator with different current density applied, distinct intrinsic resonant frequencies should occur with different currents applied. This should be the reason that the graphene—PDA actuator at a fixed size can exhibit different resonance frequencies when applying different ac densities (Figure 5b).

These intriguing and unique results may provide a basis for the design of various important and frontier actuator-based applications. Accordingly, an archetypal mini-robot with controllable direction of movement based on a graphene—PDA actuator is designed and constructed to illustrate the potential applications of this impressive actuator. The mini-robots could be fabricated through a graphene—PDA bimorph paper with asymmetrical (front-end) shapes. As an example, Figure 6 demonstrates such a mini-robot consisting of two component parts with different dimensions: the large side is about 18 mm^2, and the small side is around 8 mm^2 (Figure 6a and b). Both of the ends of the graphene—PDA actuators are connected with a flexible CNT fiber as the conductive wire. Interestingly, if fixing the frequency of the input ac, the moving direction of this mini-robot is able to be controlled through tuning the value of the input ac. For example, when applying an ac of ± 20 mA with 50 Hz frequency, the mini-robot can move from right to left (Figure 6c), while when applying an ac of ± 16 mA with 50 Hz frequency, the mini-robot can move from left to right (Figure 6d). The driving force actuating the movement of the mini-robot may be attributed to the difference of the amplitude between the oscillation of the small-dimension part and large-dimension part of the graphene—PDA

actuator. As discussed above, at a fixed frequency of the ac, the graphene—PDA actuator with larger dimensions can generate resonance under the lower value of the ac. Therefore, when applying an ac of ± 20 mA with 50 Hz frequency, the component part with relatively small dimensions of the graphene—PDA paper can match the resonance conditions and thus generate resonance, which results in producing a larger amplitude than that of the large-dimension part. The difference in amplitude between the oscillation of the small-dimension part and the large-dimension part may produce a driving force to actuate the mini-robot moving from right to left, as shown in Figure 6c. Similarly, when applying an ac of ± 16 mA with 50 Hz frequency, the large-dimension part of the graphene—PDA paper can hence generate resonance, which also leads to the production of a larger amplitude than that of the small-dimension part. Therefore, the driving force may induce the mini-robot to move back from left to right, as depicted in Figure 6d. A movie in the Supporting Information (supplementary movie 4) clearly records the whole process of the controllable movement of our mini-robot. Accordingly, if fixing a suitable value of the input ac, the moving direction of the mini-robot can also be controlled by tuning the frequency of the input ac to match the resonance frequency of the graphene—PDA actuator with different dimensions. Despite that these are only preliminary results and the graphene—PDA actuator-based mini-robot is just a prototype, it is believed that this technology and design can be exploited in a large number of advanced and practical applications through much more accurate controls.

Actuation Mechanism for the Graphene—PDA Bimorph Actuator. The interesting actuation characteristics are thought to be associated with an actuation mechanism of the graphene—PDA bimorph actuator, which fully exploits the synergism between the multifunctional properties of graphene paper and unique environmental perturbation-actuated conformation changes of PDA. It is well known that environmental stimuli, including electrical, thermal, optical, chemical, and mechanical, can actuate the conformation change of PDA chains.[15−20] In this work, it is proposed that while passing an input current through the graphene—PDA actuator, two kinds of stimuli deriving from graphene paper—the electrical field and electrothermal effect—can cause this motion of PDA chains and thus the expansion of the PDA crystal. Therefore, we consider that the actuation mechanism or the driving force for our graphene—PDA bimorph actuator is composed of two key factors. The first proposed actuation mechanism is deemed to be thermal-induced expansion of the PDA crystal. As reported by Ikehara, the linear thermal-induced expansion coefficient for the a and c axes of PDA-4U3 [R = $-(CH_2)OCONH(CH_2)_2CH_3$] crystal was larger than 1×10^{-4} K^{-1} and the crystal volume changed 1.9% between the "blue" phase and "red"
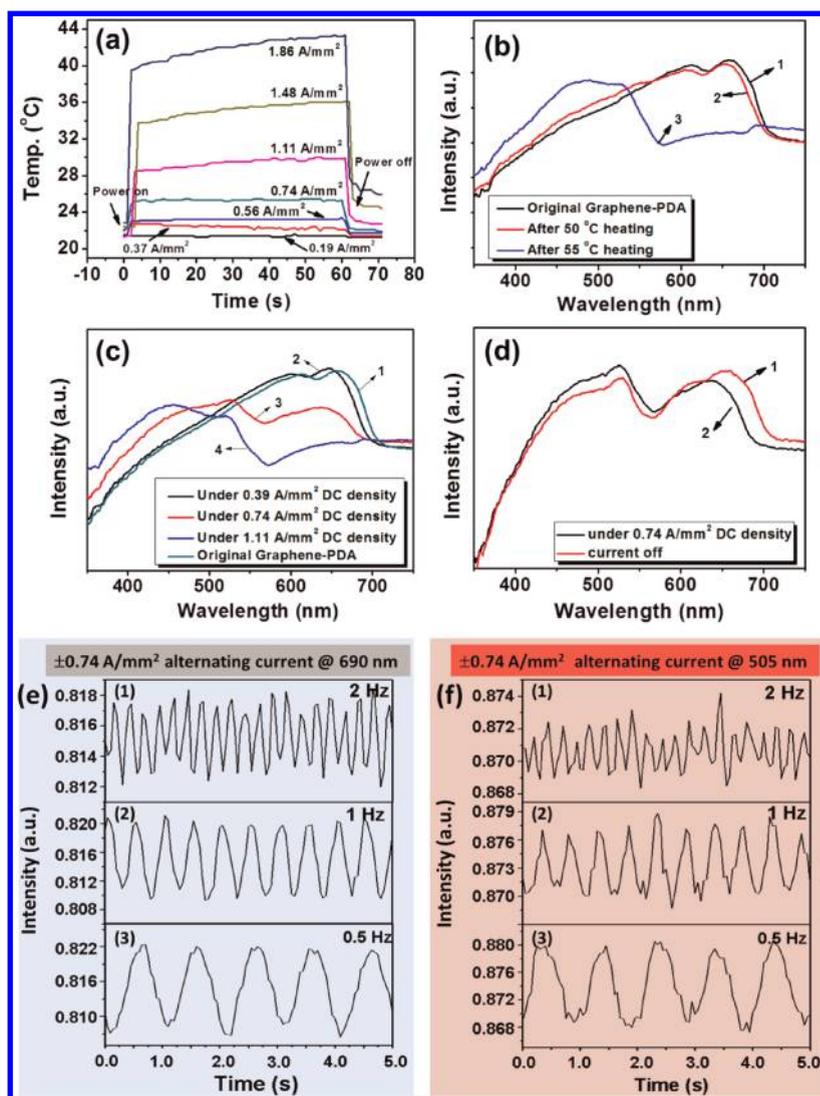
Figure 7. (a) Temperature variation of the graphene−PDA bimorph actuator at various applied dc densities from 0.19 to 1.85 A/mm^2. The temperature variation is monitored by an infrared thermometer. (b) UV−vis spectra of the as-prepared graphene−PDA actuator at room temperature (1) and respectively heated to 50 °C (2) and 55 °C (3) followed by cooling to room temperature. (c) UV−vis spectra of the as-prepared graphene−PDA actuator without applying dc (1) and respectively applying dc densities of 0.39 A/mm^2 (2), 0.74 A/mm^2 (3), and 1.11 A/mm^2 (4) while carrying out the measurement. (d) UV−vis spectra of the graphene−PDA actuator applying a dc of 20 mA (dc density about 0.74 A/mm^2) while carrying out the measurement (1) and after 20 mA dc (dc density about 0.74 A/mm^2) turned off (2). (e) UV−vis absorption vibration of the characteristic wavelength at 690 nm ("blue" phase) for the graphene−PDA actuator under ±0.74 A/mm^2 ac density with three different drive frequencies: 2 Hz (a1), 1 Hz (a2), and 0.5 Hz (a3), respectively. (f) UV−vis absorption vibration of the characteristic wavelength at 505 nm ("red" phase) for the graphene−PDA actuator under ±0.74 A/mm^2 ac density with three different driving frequencies: 2 Hz (b1), 1 Hz (b2), and 0.5 Hz (b3), respectively. All the UV−vis data are obtained from reflection values of the graphene−PDA bimorph paper and then transfered to absorption values. All measurements are carried out at room temperature, about 21 °C.

phase.[18] In the case of graphene, it has been revealed that graphite crystal has unusual thermal expansion characteristic features: a positive thermal expansion coefficient about 30×10^{-6} K^{-1} was measured in the direction perpendicular to the layer planes and a negative thermal expansion was found in the layer planes.[45] This indicates that the thermal expansion coefficient of graphene paper is smaller than that of PDA crystal.[36] Thereby, the ability of conformation change of PDA crystal induced by thermal energy is regarded as one key role in driving the actuation.

To investigate this thermal-induced actuation mechanism, the temperature variation of the graphene−PDA bimorph actuator at various applied dc density was measured, as shown in Figure 7a. The temperature of the actuator rises immediately and dramatically to a steady state as the electric power is turned on at ambient conditions. It is also found that the steady-state temperature of the actuator increases as the input dc density increases. Furthermore, the temperature variation is quite homogeneous across the whole area of the bimorph actuator, as can be seen from the

color contour plots of the temperature profile for the graphene−PDA actuators in Figure S5 (Supporting Information). It is believed that due to the remarkable thermal and electrical conductivity of graphene, the electric power can be absorbed by the graphene paper and then transferred into thermal energies to heat the actuator system.[36] This temperature rise would lead to a much larger dimension expansion of the PDA layer than that of the graphene part, and thus bring out the actuation bending phenomenon (Scheme S4). It is important to note that the actuator system also cools very fast, and theh temperature falls to room temperature promptly when the electric power is turned off (Figure 7a), which should be attributed to the extremely high thermal conductivity of graphene.[23,36] This temperature variation rate in response to the change of electric power for our graphene−PDA actuator is much higher than that of the reported polymer−CNT bimorph actuators,[42] which could give our graphene−PDA actuator a much faster response rate.[42] In addition, as depicted in Figure 2g, the curvature of the graphene−PDA actuator does not have a linear relationship with applied dc, and the curvature−current curve can be divided into three regions. The curvature coefficient for the graphene−PDA actuator (the change of curvature divided by the change of applied current) in region II is larger than that in region I and region III. This phenomenon is also consistent with the thermal-induced expansion behavior of PDA crystal.[18] It has been reported that the PDA crystal exhibits a coefficient of linear thermal expansion in the "blue" phase under relatively low temperature (region I) and can display a larger strain when the temperature is high enough to actuate the phase transition from the "blue" phase to the "red" phase (region II)[18] and then show a small coefficient of linear thermal expansion again in the "red" phase (region III) after the phase change. Consequently, the thermal-triggered expansion of PDA crystal is believed to be one of the important actuation mechanisms driving the graphene−PDA bimorph actuator.

However, the reasons behind the interesting fast and reversible oscillation actuation under high ac frequencies as displayed in Figures 5 and 6 may not only be the thermal-induced actuation mechanism. It is known that conventional thermal bimorph actuators[34,42] or electrothermal actuators,[43,44] which are composed of two materials with different thermal-induced expansion coefficients, can also exhibit rapid swing motion actuation when applying an ac with low frequencies. However, at high frequencies (usually higher than 10 Hz),[44] the cooling and heating rate of the actuator system will seriously lag the rate of current change, and thus the actuator will achieve a balanced temperature and maintain this constant value; thereby, no swing motion actuation could be observed as a result of no temperature variation.

So, another triggering mechanism may play a role in our graphene−PDA bimorph actuators, and we consider that this second actuation mechanism may be an electric-induced expansion of PDA crystal. Recently, variable range hopping conduction has been observed for graphene sheets.[46,47] Thus, as reported by previous works,[17,20] the electric field deriving from graphene paper might result in polarization of the COOH groups in the side chains of PDA. The repulsive Columbic interaction developed on the head groups of the side chains of PDA due to the polarization of COOH head groups must rearrange to accommodate a new charge distribution and thereby actuate the conformation changes of the side chains and decrease the overlap of the π-orbitals within the conjugated backbone of PDA, which not only results in the color changes of PDA but also leads to expansion of the PDA crystal.[17,20]

To confirm this mechanism of electric-induced expansion of PDA crystal, we have studied the UV−vis spectrum and color changes of graphene−PDA bimorph actuators applying different current densities and frequencies. While PDA is a traditional thermochromatic conjugated polymer, it can be seen from Figure 7b that the thermally triggered color change from blue to red of the graphene−PDA actuator should begin at a temperature higher than 50 °C (about a 30-degree increase from room temperature). By comparison, under the same environment, the electrical-induced color change of the graphene−PDA paper starts even when applying an applied dc density of about 0.39 A/mm^2 and continues under an applied dc density of 0.74 A/mm^2 (Figure 7c and Figure 2c). It is important to note that the temperature of the graphene−PDA actuator is increased by only 4 °C (from 21 to 25 °C) when applying a dc density of 0.74 A/mm^2 (Figure 7a and Figure S6). Thus, we argue that while the thermal-induced expansion of PDA crystal is one of the actuation mechanisms, the dominant one should be the electric-induced expansion of PDA crystal when applying dc and low-frequency ac.

Furthermore, while the thermochromatism is totally irreversible (Figure 7b) as observed before,[20] the electrical-induced color change of graphene−PDA bimorph paper is partially reversible, as presented in Figure 7d. In addition, this partially reversible color change of graphene−PDA paper can respond to ac at a fast speed (up to 2 Hz) and is demonstrated in Figure 7e and f, where the absorption intensity for the two characteristic peaks at 690 nm (representing the "blue" phase) and 505 nm (standing for the "red" phase) of PDA change with respect to the frequencies of input ac. Furthermore, as shown in Figure 7e and f, the peak intensity responding frequencies of PDA are double that of the input ac up to 2 Hz. The fact that the color changes with a doubled frequency indicates that the actuator or PDA responds to the current symmetrically in both current directions, and the ac in both directions

can induce the same motion of the molecular chain of PDA crystal. This double frequency absorption vibration output of PDA is consistent with the swing movement of the graphene—PDA when applying a low-frequency ac, as discussed above in Figure 4c. However, at higher frequencies, no clear spectrum change could be observed, which should be due to the slower response of the UV—vis instrument. Consequently, it is suggested that when applying a high-frequency ac, the dominant mechanism for our graphene—PDA bimorph actuators should also be the electric-induced actuation mechanism: while the graphene—PDA bimorph actuator is exposed to high-frequency ac, the high-rate conformational changes of PDA can be induced by a fast electron-hopping process under high-frequency ac charge flow. However, more work is still needed to further investigate this actuation mechanism.

CONCLUSION

In summary, a novel graphene—PDA bimorph actuator is designed and constructed utilizing a simple yet versatile method. The use of external stimuli-induced conformation changes of PDA crystal in a novel way and the effective combination of the respective unique features of PDA and graphene provide an impressive actuation performance, superior to that of conventional electromechanical actuators. The distinctive and dominant electric-induced deformation as well as the secondary thermal-induced expansion of PDA is proposed to be the main mechanism causing the high actuation performance of the flexible graphene—PDA actuator. This graphene—PDA bimorph actuator is able to be driven at low dc, and rapid swing behavior can be observed while applying an ac of high frequency. Furthermore, when the frequency and the value of the applied ac and the state of the actuators reach an appropriate level, a strong resonance can be generated. Finally, a working device consisting of a mini-robot based on graphene—PDA paper is demonstrated. Given many of the excellent properties of graphene and PDA materials and the unique actuation mechanism, this new graphene—PDA bimorph actuator and design may contribute to increase interest in practical actuation applications of graphene, such as for ultrafast switches, artificial muscle, microrobotics, optical display, prosthetic devices, and microscopic pumps.

METHODS

Raw Materials. Graphite with a particle size of 20 μm was obtained from Qingdao Huarun Graphite Co., Ltd. Hydrazine hydrate (80%) was purchased from Tianjin Ruijinte Chemical Co., Ltd. 10,12-Pentacosadiynoic acid monomer [CH$_3$-(CH$_2$)$_{11}$C≡C—C≡(CH$_2$)$_8$COOH] was purchased from Alfa Aesar Co., Ltd. and used as received.

Preparation of Graphene Papers. Graphene paper was fabricated through vacuum filtration of a graphene dispersion according to a previous report.[32] In a representative procedure, 25 mg of graphene oxide (GO), prepared from natural graphite by the modified Hummer's method,[48,49] was first completely exfoliated down to individual GO sheets in 100 mL of distilled water to form a stable dispersion of GO solution (0.25 mg/mL). Then 50 μL of hydrazine hydrate (80%) and 350 μL of ammonia solution (25%) were added to the above homogeneous solution and vigorously stirred for a few minutes. After that, the dispersion was reduced by heating to 95 °C for 1 h. Graphene paper was then obtained by filtration of the above black solution via an Anodisc membrane filter (47 mm in diameter, 0.2 μm pore size; Whatman), followed by air drying and peeling from the filter. Subsequently, the obtained paper was annealed at 400 °C in argon for 2 h for further reduction. The thickness of the graphene paper was about 10 μm. All the graphene papers were cut to desired dimensions before coating with pentacosadiynoic acid monomers.

Fabrication of Graphene—PDA Bimorph Actuator. In order to prepare the graphene—PDA bimorph actuator, the 10,12-pentacosadiynoic acid monomer was first dissolved in tetrahydrofuran at a concentration of 10 mg/mL. Then, this monomer solution was coated on one surface of the graphene paper, followed by evaporation of solvent at room temperature. The bimorph paper was covered by tin foil during the evaporation and crystallization process to prevent polymerization owing to the light exposure. After drying in air for about 24 h, the still black graphene/monomer paper was exposed to 254 nm UV radiation and polydiacetylene was formed through 1,4-addition polymerization of the 10,12-pentacosadiynoic acid monomer. The polymerization time was 1.5 min for all samples. After that, the surface of the PDA crystal side of the graphene—PDA bimorph paper became dark blue. The content of PDA in the graphene—PDA bimorph actuator can be modulated through controlling the amount of monomer solution coated on the graphene paper. As shown in Table 1, a series of graphene—PDA bimorph actuators with different loadings of PDA was prepared for comparison and investigation. Graphene—PDA-1, graphene—PDA-2, and graphene—PDA-3, whose dimensions are about 25 mm × 4 mm (length × width) with a thickness of around 10—13 μm, are used for the measurement of electric-induced stress. Graphene—PDA-4, graphene—PDA-5, graphene—PDA-6, and graphene—PDA-7, whose dimensions are about 10 mm × 2.7 mm (length × width) with a thickness of around 10—13 μm, are utilized for the measurement of actuation bending performance under different applied alternating current.

Characterization. Scanning electron microscopy (SEM) was performed on a LEO 1530 VP field emission scanning electron microscope with an acceleration voltage of 5—10 kV. The UV—vis spectra were obtained with a JASCO V-570 spectrometer in the 200—800 nm range adjusted for the background. All the UV—vis data were obtained from the solid reflection value of the graphene—PDA bimorph paper and then transfer to the absorption value. All measurements are carried out at room temperature, about 21 °C. X-ray diffraction (XRD) measurements were carried out using a Rigaku D/Max-2500 diffractometer with Cu Kα radiation. The temperature data were measured with a laser sight infrared thermometer with a resolution of 0.1 °C, and the temperature data were obtained from the graphene surface of the bimorph paper. The direct current was applied using a direct current regulated power supply, and the altering current was applied using a signal generator, which can alter the frequency from 1 μHz to 5 MHz.

Measurement of Bending Performance for the Actuator. An experimental actuator setup, as demonstrated in Figure 2a and c, was designed and used to measure the electric-induced bending performance of the actuators. One end of the length of the graphene—PDA bimorph paper was fixed to an electrode of Cu wire; the other end of the paper was connected to a flexible conductive CNT fiber, which was prepared according to the previous report.[50] When the graphene—PDA actuator was

exposed to direct current or alternating current, the end joined with the CNT fiber can move and bend freely. An optical microscope coupled with a CCD camera and high-speed camera (Casio EX-ZR100) was used to record the bending displacement and the sine wave oscillation of the graphene—PDA bimorph actuator. The bending degree of the graphene—PDA bimorph actuator is quantitatively expressed by the curvature, and the curvature can be calculated by means of the method mentioned in ref 35.

Measurement of the Electric-Induced Stress of the Actuator. An experimental actuator setup, as demonstrated in Figure S4, was designed and used to measure the electric-induced stress of the actuator. One end of the length of the graphene—PDA bimorph paper was connected to one tip of the Cu wire, with the other tip anchored on an adjustable inching lab jack; the opposite end of the actuator paper was also connected with one tip of the Cu wire, whose other tip was attached to the pan of a precision balance (over 1 of 10 000 level, Sartorius). When voltage was applied to the graphene—PDA actuator, the weight readings displayed through the precision balance changed. The electric-induced stress of the graphene—PDA actuator is dependent on both the thickness of the graphene—PDA paper and the change of weight and can be directly calculated from these two data. Before performing the actuation stress test for all actuator samples, the inching lab jack was tuned to preload a force of about 0.0196 N on the graphene—PDA papers to make sure that the papers were vertical to the horizontal plane of the balance.

Conflict of Interest: The authors declare no competing financial interest.

Supporting Information Available: Schematic illustration of PDA, characterization of graphene paper, figure of experimental setup used for the measurement of electric-induced stress, color contour plots of the temperature profile, and temperature variation for graphene—PDA actuators, and movies that recorded the quick and reversible movement, resonance for graphene—PDA actuators, and controllable archetypal mini-robot-based graphene—PDA actuators. This information is available free of charge *via* the Internet at http://pubs.acs.org.

REFERENCES AND NOTES

1. Baughman, R. H.; Cui, C. X.; Zakhidov, A. A.; Iqbal, Z.; Barisci, J. N.; Spinks, G. M.; Wallace, G. G.; Mazzoldi, A.; De Rossi, D.; Rinzler, A. G.; *et al*. Carbon Nanotube Actuators. *Science* **1999**, *284*, 1340–1344.
2. Pelrine, R.; Kornbluh, R.; Pei, Q. B.; Joseph, J. High-Speed Electrically Actuated Elastomers with Strain Greater than 100%. *Science* **2000**, *287*, 836–839.
3. Baughman, R. H. Conducting Polymer Artificial Muscles. *Synth. Met.* **1996**, *78*, 339–353.
4. Lendlein, A.; Jiang, H. Y.; Junger, O.; Langer, R. Light-Induced Shape-Memory Polymers. *Nature* **2005**, *434*, 879–882.
5. Koerner, H.; Price, G.; Pearce, N. A.; Alexander, M.; Vaia, R. A. Remotely Actuated Polymer Nanocomposites - Stress-Recovery of Carbon-Nanotube-Filled Thermoplastic Elastomers. *Nat. Mater.* **2004**, *3*, 115–120.
6. Ahir, S. V.; Terentjev, E. M. Photomechanical Actuation in Polymer-Nanotube Composites. *Nat. Mater.* **2005**, *4*, 491–495.
7. Park, S. E.; Shrout, T. R. Relaxor Based Ferroelectric Single Crystals for Electro-Mechanical Actuators. *Mater. Res. Innovations* **1997**, *1*, 20–25.
8. Uchino, K. Materials Issues in Design and Performance of Piezoelectric Actuators: An Overview. *Acta Mater.* **1998**, *46*, 3745–3753.
9. Pelrine, R.; Kornbluh, R.; Kofod, G. High-Strain Actuator Materials Based on Dielectric Elastomers. *Adv. Mater.* **2000**, *12*, 1223–1225.
10. Ha, S. M.; Yuan, W.; Pei, Q. B.; Pelrine, R.; Stanford, S. Interpenetrating Polymer Networks for High-Performance Electroelastomer Artificial Muscles. *Adv. Mater.* **2006**, *18*, 887–891.
11. Madden, J. D.; Cush, R. A.; Kanigan, T. S.; Hunter, I. W. Fast Contracting Polypyrrole Actuators. *Synth. Met.* **2000**, *113*, 185–192.
12. Smela, E.; Lu, W.; Mattes, B. R. Polyaniline Actuators - Part 1. PANI(AMPS) in HCl. *Synth. Met.* **2005**, *151*, 25–42.
13. Lu, Y. F.; Yang, Y.; Sellinger, A.; Lu, M. C.; Huang, J. M.; Fan, H. Y.; Haddad, R.; Lopez, G.; Burns, A. R.; Sasaki, D. Y.; *et al*. Self-assembly of Mesoscopically Ordered Chromatic Polydiacetylene/Silica Nanocomposites. *Nature* **2001**, *410*, 913–917.
14. Okada, S.; Peng, S.; Spevak, W.; Charych, D. Color and Chromism of Polydiacetylene Vesicles. *Acc. Chem. Res.* **1998**, *31*, 229–239.
15. Sun, X.; Chen, T.; Huang, S.; Li, L.; Peng, H. Chromatic Polydiacetylene with Novel Sensitivity. *Chem. Soc. Rev.* **2010**, *39*, 4244–4257.
16. Carpick, R. W.; Sasaki, D. Y.; Marcus, M. S.; Eriksson, M. A.; Burns, A. R. Polydiacetylene Films: a Review of Recent Investigations into Chromogenic Transitions and Nanomechanical Properties. *J. Phys.-Condens. Mater.* **2004**, *16*, R679–R697.
17. Cheng, Q.; Stevens, R. C. Charge-Induced Chromatic Transition of Amino Acid-Derivatized Polydiacetylene Liposomes. *Langmuir* **1998**, *14*, 1974–1976.
18. Ikehara, T.; Shimada, S.; Matsuda, H.; Tanaka, M. Anisotropic Thermal Strain Measurement at the Thermochromic Phase Transition in a Polydiacetylene Crystal. *Phys. Rev. B* **2001**, *64*, 092202.
19. Ikehara, T.; Tanaka, M.; Shimada, S.; Matsuda, H. Optically Driven Actuator Using Photo-Induced Phase-Transition Polymer. *Sensor. Actuat. A-Phys.* **2002**, *96*, 239–243.
20. Peng, H. S.; Sun, X. M.; Cai, F. J.; Chen, X. L.; Zhu, Y. C.; Liao, G. P.; Chen, D. Y.; Li, Q. W.; Lu, Y. F.; Zhu, Y. T.; *et al*. Electrochromatic Carbon Nanotube/Polydiacetylene Nanocomposite Fibres. *Nat. Nanotechnol.* **2009**, *4*, 738–741.
21. Geim, A. K.; Novoselov, K. S. The Rise of Graphene. *Nat. Mater.* **2007**, *6*, 183–191.
22. Novoselov, K. S.; Geim, A. K.; Morozov, S. V.; Jiang, D.; Zhang, Y.; Dubonos, S. V.; Grigorieva, I. V.; Firsov, A. A. Electric Field Effect in Atomically Thin Carbon Films. *Science* **2004**, *306*, 666–669.
23. Balandin, A. A.; Ghosh, S.; Bao, W. Z.; Calizo, I.; Teweldebrhan, D.; Miao, F.; Lau, C. N. Superior Thermal Conductivity of Single-Layer Graphene. *Nano Lett.* **2008**, *8*, 902–907.
24. Lee, C.; Wei, X. D.; Kysar, J. W.; Hone, J. Measurement of the Elastic Properties and Intrinsic Strength of Monolayer Graphene. *Science* **2008**, *321*, 385–388.
25. Meyer, J. C.; Geim, A. K.; Katsnelson, M. I.; Novoselov, K. S.; Booth, T. J.; Roth, S. The Structure of Suspended Graphene Sheets. *Nature* **2007**, *446*, 60–63.
26. Stankovich, S.; Dikin, D. A.; Dommett, G. H. B.; Kohlhaas, K. M.; Zimney, E. J.; Stach, E. A.; Piner, R. D.; Nguyen, S. T.; Ruoff, R. S. Graphene-Based Composite Materials. *Nature* **2006**, *442*, 282–286.
27. Avouris, P.; Chen, Z. H.; Perebeinos, V. Carbon-Based Electronics. *Nat. Nanotechnol.* **2007**, *2*, 605–615.
28. Dikin, D. A.; Stankovich, S.; Zimney, E. J.; Piner, R. D.; Dommett, G. H. B.; Evmenenko, G.; Nguyen, S. T.; Ruoff, R. S. Preparation and Characterization of Graphene Oxide Paper. *Nature* **2007**, *448*, 457–460.
29. Ramanathan, T.; Abdala, A. A.; Stankovich, S.; Dikin, D. A.; Herrera-Alonso, M.; Piner, R. D.; Adamson, D. H.; Schniepp, H. C.; Chen, X.; Ruoff, R. S.; *et al*. Functionalized Graphene Sheets for Polymer Nanocomposites. *Nat. Nanotechnol.* **2008**, *3*, 327–331.
30. Stoller, M. D.; Park, S. J.; Zhu, Y. W.; An, J. H.; Ruoff, R. S. Graphene-Based Ultracapacitors. *Nano Lett.* **2008**, *8*, 3498–3502.
31. Chen, H.; Muller, M. B.; Gilmore, K. J.; Wallace, G. G.; Li, D. Mechanically Strong, Electrically Conductive, and Biocompatible Graphene Paper. *Adv. Mater.* **2008**, *20*, 3557–3561.

32. Liang, J. J.; Xu, Y. F.; Sui, D.; Zhang, L.; Huang, Y.; Ma, Y. F.; Li, F. F.; Chen, Y. S. Flexible, Magnetic, and Electrically Conductive Graphene/Fe$_3$O$_4$ Paper and Its Application For Magnetic-Controlled Switches. *J. Phys. Chem. C* **2010**, *114*, 17465–17471.

33. Rogers, G. W.; Liu, J. Z. Graphene Actuators: Quantum-Mechanical and Electrostatic Double-Layer Effects. *J. Am. Chem. Soc.* **2011**, *133*, 10858–10863.

34. Shin, K. Y.; Hong, J. Y.; Jang, J. S. Flexible and Transparent Graphene Films as Acoustic Actuator Electrodes Using Inkjet Printing. *Chem. Commun.* **2011**, *47*, 8527–8529.

35. Xie, X. J.; Qu, L. T.; Zhou, C.; Li, Y.; Zhu, J.; Bai, H.; Shi, G. Q.; Dai, L. M. An Asymmetrically Surface-Modified Graphene Film Electrochemical Actuator. *ACS Nano* **2010**, *4*, 6050–6054.

36. Zhu, S. E.; Shabani, R.; Rho, J.; Kim, Y.; Hong, B. H.; Ahn, J. H.; Cho, H. J. Graphene-Based Bimorph Microactuators. *Nano Lett.* **2011**, *11*, 977–981.

37. Sungjin, P.; Jinho, A.; Ji, W. S.; Ruoff, R. Graphene-Based Actuators. *Small* **2010**, *6*, 210–212.

38. Liang, J. J.; Huang, Y.; Oh, J. Y.; Kozlov, M.; Sui, D.; Fang, S. L.; Baughman, R. H.; Ma, Y. F.; Chen, Y. S. Electromechanical Actuators Based on Graphene and Graphene/Fe$_3$O$_4$ Hybrid Paper. *Adv. Funct. Mater.* **2011**, *21*, 3778–3784.

39. Li, D.; Muller, M. B.; Gilje, S.; Kaner, R. B.; Wallace, G. G. Processable Aqueous Dispersions of Graphene Nanosheets. *Nat. Nanotechnol.* **2008**, *3*, 101–105.

40. Yang, Y.; Lu, Y. F.; Lu, M. C.; Huang, J. M.; Haddad, R.; Xomeritakis, G.; Liu, N. G.; Malanoski, A. P.; Sturmayr, D.; Fan, H. Y.; *et al.* Functional Nanocomposites Prepared by Self-Assembly and Polymerization of Diacetylene Surfactants and Silicic Acid. *J. Am. Chem. Soc.* **2003**, *125*, 1269–1277.

41. Takami, K.; Mizuno, J.; kai-Kasaya, M.; Saito, A.; Aono, M.; Kuwahara, Y. Conductivity Measurement of Polydiacetylene Thin Films by Double-Tip Scanning Tunneling Microscopy. *J. Phys. Chem. B* **2004**, *108*, 16353–16356.

42. Chen, L. Z.; Liu, C. H.; Liu, K.; Meng, C. Z.; Hu, C. H.; Wang, J. P.; Fan, S. S. High-Performance, Low-Voltage, and Easy-Operable Bending Actuator Based on Aligned Carbon Nanotube/Polymer Composites. *ACS Nano* **2011**, *5*, 1588–1593.

43. Sellinger, A. T.; Wang, D. H.; Tan, L. S.; Vaia, R. A. Electrothermal Polymer Nanocomposite Actuators. *Adv. Mater.* **2010**, *22*, 3430–3435.

44. Hu, Y.; Chen, W.; Lu, L. H.; Liu, J. H.; Chang, C. R. Electromechanical Actuation with Controllable Motion Based on a Single-Walled Carbon Nanotube and Natural Biopolymer Composite. *ACS Nano* **2010**, *4*, 3498–3502.

45. Suleimanov, R. A.; Abdullaev, N. A. The Nature of Negative Linear Expansion of Graphite Crystals. *Carbon* **1993**, *31*, 1011–1013.

46. Kim, K.; Park, H. J.; Woo, B. C.; Kim, K. J.; Kim, G. T.; Yun, W. S. Electric Property Evolution of Structurally Defected Multilayer Graphene. *Nano Lett.* **2008**, *8*, 3092–3096.

47. Gomez-Navarro, C.; Weitz, R. T.; Bittner, A. M.; Scolari, M.; Mews, A.; Burghard, M.; Kern, K. Electronic Transport Properties of Individual Chemically Reduced Graphene Oxide Sheets. *Nano Lett.* **2007**, *7*, 3499–3503.

48. Becerril, H. A.; Mao, J.; Liu, Z.; Stoltenberg, R. M.; Bao, Z.; Chen, Y. Evaluation of Solution-Processed Reduced Graphene Oxide Films as Transparent Conductors. *ACS Nano* **2008**, *2*, 463–470.

49. Hirata, M.; Gotou, T.; Horiuchi, S.; Fujiwara, M.; Ohba, M. Thin-Film Particles of Graphite Oxide 1: High-Yield Xynthesis and Flexibility of the Particles. *Carbon* **2004**, *42*, 2929–2937.

50. Zhang, M.; Atkinson, K. R.; Baughman, R. H. Multifunctional Carbon Nanotube Yarns by Downsizing an Ancient Technology. *Science* **2004**, *306*, 1358–1361.